Geophysical Research Letters

RESEARCH LETTER
10.1029/2022GL100609

Key Points:

- Pinatubo aerosol forcing is set over land and ocean respectively to investigate roles of land and ocean cooling in exciting an El Niño
- The volcano-induced land cooling, especially tropical African cooling, plays an essential role in exciting an El Niño following eruptions
- The oceanic volcanic forcing could induce a fast dipole response in the Indian Ocean, exciting a slow western Pacific El Niño-like cooling

Correspondence to:

F. Liu and C. Gao,
liufei26@mail.sysu.edu.cn;
gaocc@zju.edu.cn

Citation:

Liu, F., Xing, C., Chen, L., Gao, C., Lian, T., Zhou, S., et al. (2022). Relative roles of land and ocean cooling in triggering an El Niño following tropical volcanic eruptions. *Geophysical Research Letters*, *49*, e2022GL100609. https://doi.org/10.1029/2022GL100609

Received 1 AUG 2022
Accepted 24 NOV 2022

Author Contributions:

Conceptualization: Fei Liu, Chaochao Gao, Bin Wang, Wenjie Dong
Data curation: Fei Liu
Formal analysis: Fei Liu, Hui Wang
Funding acquisition: Fei Liu, Wenjie Dong
Investigation: Fei Liu, Lin Chen, Tao Lian, Hui Wang, Bin Wang, Wenjie Dong
Methodology: Fei Liu, Chen Xing, Chaochao Gao, Shangrong Zhou, Hui Wang, Wenjie Dong
Project Administration: Fei Liu, Wenjie Dong
Resources: Fei Liu, Chen Xing
Software: Fei Liu, Chen Xing, Hui Wang
Supervision: Fei Liu, Bin Wang, Wenjie Dong
Validation: Fei Liu, Chen Xing

Relative Roles of Land and Ocean Cooling in Triggering an El Niño Following Tropical Volcanic Eruptions

Fei Liu[1,2], Chen Xing[3], Lin Chen[2,4], Chaochao Gao[5], Tao Lian[6], Shangrong Zhou[1], Hui Wang[1], Bin Wang[7], and Wenjie Dong[1]

[1]School of Atmospheric Sciences, Key Laboratory of Tropical Atmosphere-Ocean System Ministry of Education, Southern Marine Science and Engineering Guangdong Laboratory, Sun Yat-sen University, Zhuhai, China, [2]Collaborative Innovation Center on Forecast and Evaluation of Meteorological Disasters (CIC-FEMD), Nanjing University of Information Science and Technology, Nanjing, China, [3]Bren School of Environmental Science & Management, University of California, Santa Barbara, Santa Barbara, CA, USA, [4]Key Laboratory of Meteorological Disaster Ministry of Education (KLME), School of Atmospheric Sciences, Nanjing University of Information Science and Technology, Nanjing, China, [5]College of Environmental and Resource Sciences, Zhejiang University, Hangzhou, China, [6]State Key Laboratory of Satellite Ocean Environment Dynamics, Second Institute of Oceanography, Hangzhou, China, [7]Department of Atmospheric Sciences, Atmosphere-Ocean Research Center, University of Hawai'i at Mānoa, Honolulu, HI, USA

Abstract Paleoclimate evidence suggests that tropical volcanic eruptions could increase the likelihood of El Niño occurrence. Previous numerical model studies with zonally uniform volcanic aerosol forcing suggested the roles of land cooling-induced monsoon suppression and ocean cooling-induced air-sea interaction in triggering an El Niño following the eruption. Here, we perform targeted sensitivity experiments by confining aerosol forcing over land or ocean only in the fully coupled Community Earth System Model to assess relative roles of these land and ocean cooling. Our results indicate that volcanic aerosol over land, especially over the large landmass of tropical Africa, is more effective in exciting an El Niño than over ocean. The suppressed African monsoon excites Kelvin-wave westerly wind anomalies over the tropical central Pacific, triggering an El Niño through the Bjerknes feedback. Under the uniform ocean aerosol forcing, the Indian Ocean's fast dipole response induces a slow western Pacific El Niño-like cooling in the second year.

Plain Language Summary Paleoclimate analyses suggest that tropical volcanic eruptions can increase the likelihood of El Niño. Scientists performed numerical model experiments with zonally uniform aerosol forcing to understand this phenomenon. Two triggering mechanisms have been proposed. One emphasizes the role of land cooling that could suppress monsoon, inducing westerly wind anomalies and triggering an El Niño. The other stresses the role of ocean cooling-induced atmosphere-ocean interaction (ocean dynamical thermostat mechanism) in generating an El Niño. Previous works could not answer which one is more important in exciting an El Niño since these two mechanisms happen simultaneously in their simulations. We perform a suite of sensitivity experiments to address this question by setting volcanic aerosol over land and ocean separately. Our simulations suggest that the fast land cooling-induced land-sea thermal contrast and tropical monsoon suppression, especially the tropical African monsoon suppression, are more critical in exciting an El Niño than the overall ocean cooling. The latter can only excite a western Pacific El Niño-like cooling.

1. Introduction

El Niños were observed following four out of the five large tropical volcanic eruptions over the past 150 years, which are 1902 Santa Maria eruption, 1963 Agung eruption, 1982 El Chichón eruption, and 1991 Pinatubo eruption, except for 1883 Krakatau eruption, suggesting the linkage between tropical eruptions and the following El Niños (Handler, 1984; Khodri et al., 2017; Liu et al., 2020; Mcgregor et al., 2020; Xing et al., 2020). This temporal linkage was also reported in paleoclimate analyses (Adams et al., 2003; D'Arrigo et al., 2009; Liu et al., 2018; 2022; Mcgregor et al., 2010, 2020; Robock, 2020; Wilson et al., 2010), although some reconstruction results, especially based on fossil corals from the central tropical Pacific, disapproved of such linkage that tropical eruptions can increase the likelihood of El Niño (Dee et al., 2020; Zhu et al., 2022).

Numerical model simulations have been performed to understand this linkage between tropical eruptions and the following El Niños due to their good performance in simulating the El Niño evolution and climatic responses after

Visualization: Fei Liu, Lin Chen, Chaochao Gao, Tao Lian, Bin Wang, Wenjie Dong
Writing – original draft: Fei Liu, Chaochao Gao, Bin Wang, Wenjie Dong
Writing – review & editing: Fei Liu, Lin Chen, Chaochao Gao, Tao Lian, Shangrong Zhou, Hui Wang, Bin Wang, Wenjie Dong

tropical volcanic eruptions (F. S. R. Pausata et al., 2020; Khodri et al., 2017; Lim et al., 2016; Liu et al., 2018; Maher et al., 2015; Mann et al., 2005; Ohba et al., 2013; Predybaylo et al., 2017, 2020; Stevenson et al., 2017; Wilson et al., 2010). Based on these simulation studies, the mechanisms of tropical eruption exciting an El Niño can be generally separated into two groups: the ocean cooling related and the fast land cooling triggered.

Under overall tropical cooling after eruptions, an El Niño could develop through the ocean dynamical thermostat mechanism (Maher et al., 2015; Mann et al., 2005; Predybaylo et al., 2017). The mechanism suggests that the reduced ocean surface heating cools sea surface temperature (SST) more in the western Pacific (Clement et al., 1996), because in the eastern Pacific the reduced heating will weaken the cooling caused by the upwelling-induced vertical advection of cold water. The reduced zonal SST gradient gives rise to a reduced pressure gradient and hence weaker easterly winds, which in turn further reduce the SST gradient, a mechanism known as the Bjerknes feedback (Bjerknes, 1969). The volcanic eruption-induced cooling also reduces evaporation in the cloudless subtropical region and weakens the Intertropical Convergence Zone, which result in a weakening of the trade winds, leading to an El Niño (Lim et al., 2016). These volcanic eruption-induced El Niño/South Oscillation (ENSO) responses differ following individual eruptions, depending on the initial ocean conditions (Predybaylo et al., 2017, 2020), which may explain why the 1883 Krakatau eruption was not followed by an El Niño event.

The land, having less heat capacity, cools faster than the ocean in response to tropical eruptions; thus, the reduced evaporation and land-sea thermal contrast decrease the rainfall over the Maritime Continent (Chai et al., 2020; Ohba et al., 2013) and weaken the West African monsoon (Khodri et al., 2017). The reduced convection excites equatorial westerly anomalies over the Pacific due to the Kelvin wave propagation in Gill response (Gill, 1980; Matsuno, 1966). The El Niño develops subsequently through the Bjerknes feedback. These analyses, however, were performed based on the zonally uniform volcanic aerosol forcing, and the roles of ocean cooling and fast land cooling were hard to be a distinctive diagnosis.

Using the atmospheric component of Institut Pierre Simon Laplace (IPSL)-CM5B model and changing the land surface albedo to mimic the role of aerosol forcing over land, Khodri et al. (2017, hereafter Kh17) found that the tropical African cooling is the leading factor in exciting an El Niño after the tropical eruption. The equatorial Pacific SST response to the simulated wind anomalies was estimated separately by forcing a linear ocean model (Kh17). The leading role of Maritime Continent cooling in exciting the El Niño, however, was found by Chai et al. (2020). In their work, the land cooling response to volcanic eruptions was mimicked by increasing the land surface albedo in the coupled Community Earth System Model (CESM). It is unclear whether the Kh17 and Chai et al. (2020) conclusions are model-dependent or method-dependent. To investigate relative roles of ocean cooling and fast land cooling in exciting an El Niño, we use the fully coupled model, the CESM version 1.2 (CESM1.2), and perform different sensitivity experiments by setting volcanic aerosol forcing over land and ocean separately.

2. Data and Methods

The coupled CESM1.2 is used in this work due to its good simulation of ENSO in terms of seasonality, frequency, and associated teleconnection (Bellenger et al., 2014; Capotondi et al., 2020) and the ability to simulate El Niño response to large tropical eruptions (Liu et al., 2018, 2022; Stevenson et al., 2016, 2017; Yang et al., 2022), although the internal ENSO variation is stronger than observation (Stevenson et al., 2016). The atmosphere model is Community Atmosphere Model version 5.0 (CAM5) and is coupled with the Parallel Ocean Program version 2 (POP2) and the Community Land Model version 4.0. More details of CESM1.2 can be found in Kay et al. (2015). The horizontal resolution is 1.9° (latitude) × 2.5° (longitude) for CAM5. In POP2, approximately 1° resolution (384 latitude grids × 320 longitude grids) is used. The vertical resolutions are 26 and 60 levels for the atmosphere and ocean components, respectively.

A 150-year run is performed initializing from the by-default present day condition, in which greenhouse gas concentration, aerosol and ozone forcing, as well as solar variability were all fixed at their 2000 values. Based on the same forcing, we run an additional 100-year control run for large ensemble simulation to use macro perturbation (Hawkins et al., 2016). From this 100-year control run every fifth year is used as the 20 different initial conditions for the fully coupled sensitivity experiments with only changing the spatial pattern of volcanic forcing. We then perform three sets of 20-ensemble sensitivity experiments with volcanic aerosol over land, ocean,

Table 1
Details of Control Run and Sensitivity Experiments With Volcanic Aerosol Forcing Over Different Land and Ocean Regions in CESM1.2

Experiments	Ensemble size	Volcanic forcing	Forcing area	Over land or ocean
Control	20	No	–	–
Global	20	Yes	90°S–90°N and 0°–360°	Land and ocean
Land-global	20	Yes	90°S–90°N, 0°–360°	Land
Ocean-global	20	Yes	90°S–90°N, 0°–360°	Ocean
Land-tropics	20	Yes	23.5°S–23.5°N, 0°–360°	Land
Land-extratropics	20	Yes	90°–23.5°S, 23.5°–90°N, 0°–360°	Land
Land-trop Asia-AUS	20	Yes	23.5°S–23.5°N, 70°–154°E	Land
Land-trop Africa	20	Yes	23.5°S–23.5°N, 20°W–52°E	Land
Land-trop America	20	Yes	23.5°S–23.5°N, 120°–30°W	Land

and both (Table 1). An ensemble of 3-year experiments is started from January of each initial year. Five sets of additional land sensitivity experiments with volcanic aerosol over extratropical, whole tropical, tropical African, tropical American, and tropical Asian-Australian (including Maritime Continent) lands are also performed, and definitions of these regions are listed in Table 1.

To isolate the volcanic impact and remove internal variability, composite of large ensembles has usually been used (Clyne et al., 2021; F. S. Pausata et al., 2015; F. S. R. Pausata et al., 2016; Stevenson et al., 2017; Zanchettin et al., 2013), and 20 ensembles are used for each set of experiments in this work. Ensemble mean of these 20 control runs doesn't show significant ENSO signal, that is, no significant Niño3.4 index anomaly with respect to climatological annual cycle (not shown). Differences in the ensemble mean with and without the volcanic forcing are used to quantify the volcanic effect. Significant signals are detected by the Student's *t*-test, for which the confidence intervals are calculated by the paired *t*-test for the anomalies between these sensitivity experiments and control run.

Similar to Kh17, we choose Pinatubo eruption in June 1991 as an example, since it is the best documented tropical eruptions with climatically significant stratospheric aerosol injection. The volcanic aerosol forcing data is from Ammann et al. (2003), which has been used in CESM Large Ensemble and Coupled Model Intercomparison Project Phase 5 historical simulations therefore facilitates cross-model comparison (Kay et al., 2015; Taylor et al., 2012; Xing et al., 2020). Ammann et al. (2003) Pinatubo forcing is slightly larger than that in Sato et al. (1993) reconstruction, and tends to distribute more aerosols in Northern Hemisphere middle latitude during the second year than Gao et al. (2008) and Toohey and Sigl (2017) reconstructions (not shown). Each sensitivity experiment lasts 3 years, forced by this Pinatubo eruption forcing from 1991 to 1993.

Difference in magnitude and spatiotemporal distribution of the volcanic cloud, however, does not change our results qualitatively, as we are focusing on the relative roles of land versus ocean-cooling responses to external forcing. Pinatubo eruption is large enough to excite the ENSO response, and threshold of volcanic magnitude that leads to the El Niño-like response, as presented by Lim et al. (2016), is not focused here. Although our results will show weak impact of extratropical aerosol forcing on ENSO response, the updated volcanic forcing for CMIP6 or Model Intercomparison Project on the climate response to Volcanic forcing project (VolMIP) simulations (Thomason et al., 2018), presenting different meridional aerosol distributions from Ammann et al. (2003), will be investigated in the near future.

Relative SST, defined as SST minus the tropical (20°S–20°N) mean SST, is used to calculate the relative Niño3.4 index (Khodri et al., 2017; Robock, 2020), which has been suggested to be much helpful for analyzing essential ENSO variation under the volcano-induced tropical cooling. The positive phase of relative Niño3.4 index represents the western Pacific El Niño-like cooling, a tropical Pacific cooling response that mainly occurs in western Pacific while central-to-eastern tropical Pacific remains neural or weak warming.

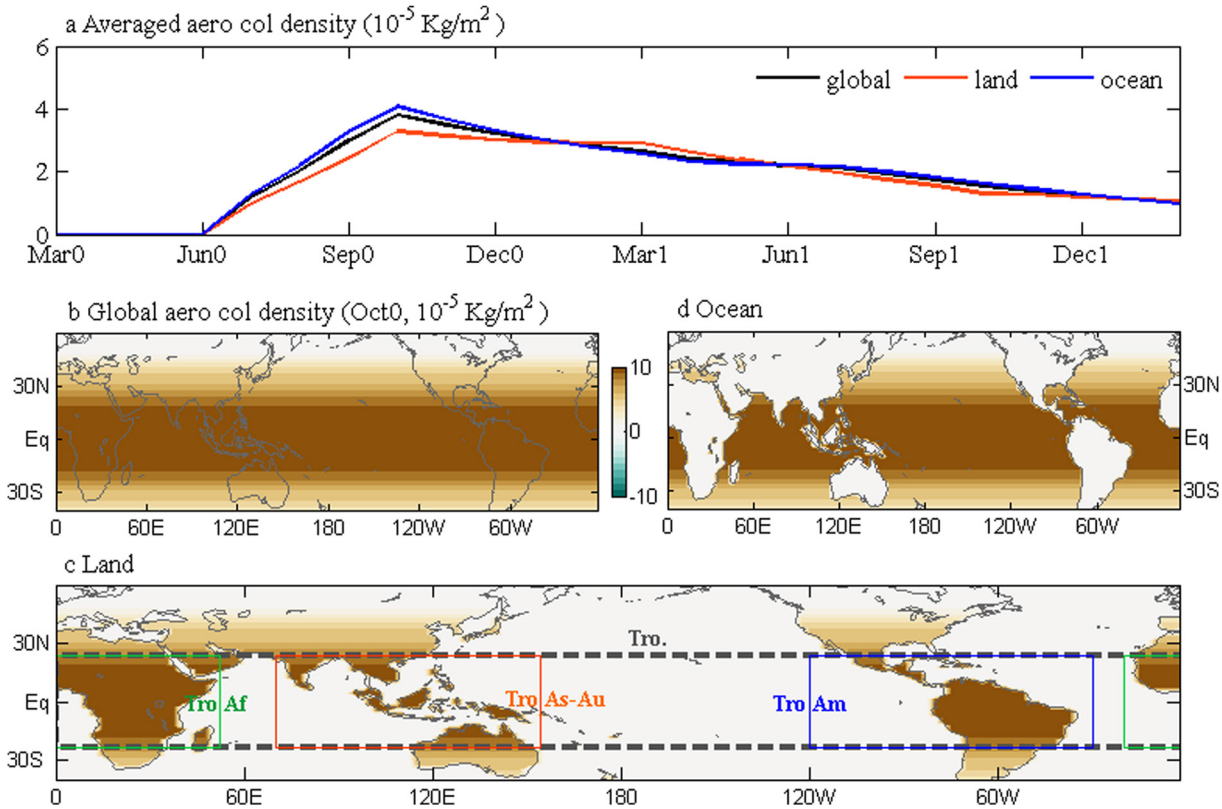

Figure 1. Different volcanic aerosol forcings over land and ocean. Shown are (a) aerosol column density evolution and the horizontal distribution over (b) global, (c) global land, and (d) global ocean in October 1991, reconstructed by Ammann et al. (2003). In panel (c) gray (all tropical), orange (tropical Asian-Australian), blue (tropical American), and green (tropical African) boxes denote different tropical land regions, as listed in Table 1.

3. Results and Discussions

The 1991 Pinatubo volcano eruption over Philippines injected a large amount of sulfur gas into stratosphere. The formed sulfur aerosol peaked during the fall with a global average of about 3.9×10^{-5} kg/m^2, then decayed linearly to a half of its strength 1 year later (Figure 1a). For a tropical eruption, the stratospheric forcing of Pinatubo displays a symmetric distribution to the equator during the eruption year. The aerosol column density reaches 9.0×10^{-5} kg/m^2 at the equator and decays poleward for the peak forcing period in October 1991 (Figure 1b). The aerosol forcing exhibits a uniform zonal distribution because of strong zonal wind transportation in the stratosphere. Figures 1c and 1d show the aerosol forcings over land and ocean, respectively, which have similar amplitudes.

The ENSO response excited by global volcanic forcing, represented by the composite difference of Niño3.4 index between Global scenario and CTL experiments, first displays a decreasing trend that peaks in October of the eruption year (hereafter referred to as Oct0, same for the other post eruption months) with a negative anomaly of −0.15 K (Figure 2a). After a very weak increase during the following winter and spring, the Niño3.4 response increases quickly after Jun1 and peaks at Oct1 with a significant positive value of 1.2 K. This result means that an El Niño can be excited 1 year after the peak aerosol forcing in CESM1.2. The simulated El Niño 1 year after the Pinatubo or other tropical volcanic forcing was also found by previous simulations in CESM (Liu et al., 2018; Stevenson et al., 2016, 2017; W. Sun et al., 2019). The large ensemble spread is due to different initial oceanic conditions, with larger El Niño response for an initial El Niño developing condition than for a La Niña condition (not shown), in consistent with previous finding (Predybaylo et al., 2017, 2020). In the following discussion we will focus on the ensemble mean while neglect the role of initial condition.

When aerosol forcing is prescribed only over land, CESM1.2 can simulate significant positive Niño3.4 response since boreal winter of the eruption year (hereafter referred to as Winter0, same for the other post eruption seasons), which increases to a peak of 0.9 K in Nov1 and then decreases (Figure 2a). The simulated Niño3.4 response under

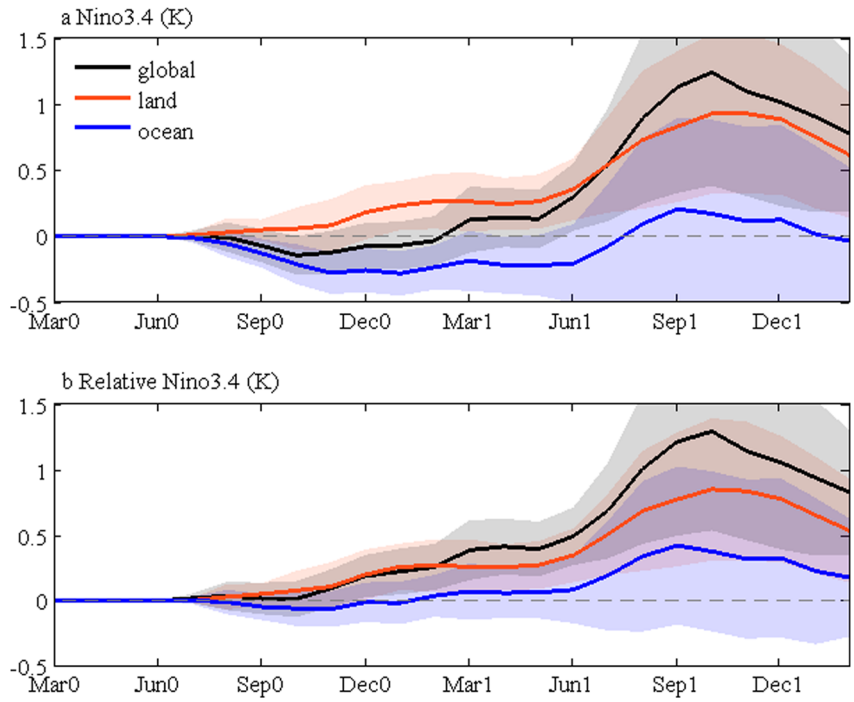

Figure 2. Simulated El Niño/South Oscillation responses to different volcanic forcing. (a) Ensemble average (20 ensembles) of Niño3.4 (5°S–5°N and 170°W–120°W) sea surface temperature (SST) responses (°C; represented by the differences between sensitivity experiments with volcanic forcing and CTL run without volcanic forcing) to the 1991 Pinatubo aerosol forcing over global (black line), land (orange line), and ocean (blue line) from March of the eruption year to 23 months later. Shading shows the 95% confidence intervals of the change seen in all experiments calculated by Student's *t*-test. "0" and "1" denote the eruption year and the first post-eruption year, respectively. Panel (b) same as panel (a) except for the relative Niño3.4 SST responses with respect to tropical (20°S–20°N) average.

the Land scenario turns positive earlier and reaches a peak value that is a little weaker than that under the Global scenario. The Ocean scenario, however, cannot simulate significant positive Niño3.4 response after the eruption. Instead, the Niño3.4 response turns negative and reaches peak value of −0.28 K in Nov0, which could have contributed to the overall negative response during the eruption year in the Global scenario.

The fast decrease in Niño3.4 response concurs with the maximum volcanic aerosol forcing during Sep0–Nov0 in the Ocean scenario (Figure 1a). To isolate the role of ocean dynamics under the volcanic-induced tropical cooling, the relative Niño3.4 index with respect to tropical (20°S–20°N) average SST is investigated, following previous works (Khodri et al., 2017; Robock, 2020). After removing volcanic cooling effect, the negative anomalies in the relative Niño3.4 index for both Global and Ocean scenarios mostly disappear (Figure 2b). Significant positive anomalies are simulated since Winter0 for both Global and Land simulations and peak in Autumn1. Under the Ocean scenario, the relative Niño3.4 anomaly is very weak during the first 12 months after eruptions, which then becomes positive and peaks around Sep1, although this response is still not significant. The Land and Ocean-only responses contribute roughly 2/3 and 1/3 to the peak global relative Niño3.4 response at Nov1, respectively (Figure 2b).

These results show that an El Niño can be simulated when volcanic aerosols are over or only over land. During the eruption year, the Global scenario shows a western Pacific El Niño-like cooling response, demonstrated by a positive relative Niño3.4 while negative raw Niño3.4 response. The aerosol forcing over land contributes to the El Niño-like response, while that over ocean mainly contributes to the cooling. During the second year the ocean dynamic response, represented by positive relative Niño3.4 anomaly, starts to work and tends to reinforce the land cooling-induced El Niño response.

The strong El Niño response to aerosol forcing over land is mainly induced by the forcing over tropical region rather than over extratropical region, as indicated by the neutral Niño3.4 response under the Land-Extratropical scenario (not shown). Under the Land-Tropical scenario, the tropical monsoon precipitation is suppressed

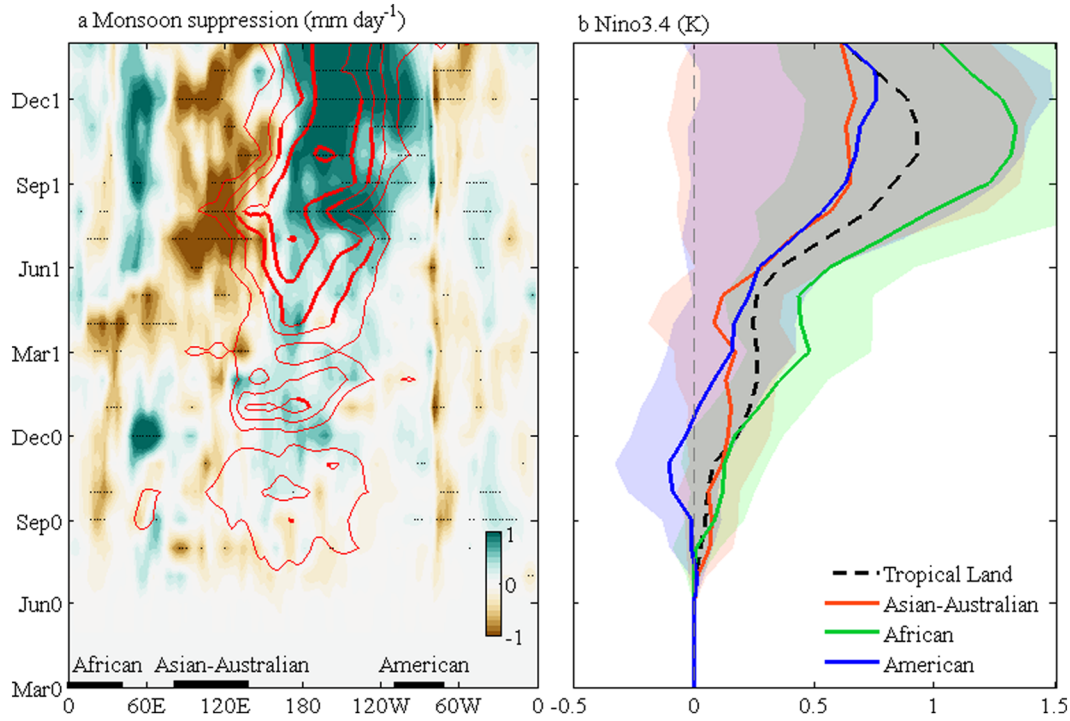

Figure 3. Role of land volcanic forcing in El Niño excitation. (a) Hovmöller diagram of tropical (10°S–10°N) precipitation anomalies (shading, mm/day) and 850-hPa zonal wind anomalies (contour, m/s) that respond to tropical land aerosol forcing. Red contours denote positive zonal wind anomalies, respectively, and contour interval is 0.5 m/s. Zero contour is not shown. Stippling and thick line denote anomalies significant at 95% confidence level based on the Student *t*-test. Panel (b) same as in Figure 2a except for the volcanic forcing over tropical land (black dashed), tropical Asian-Australian region (orange), tropical Africa (green), and tropical America (blue).

quickly from Aug0 and the most significant suppression occurs over the tropical African and American regions (Figure 3a). At the same time, westerly wind anomaly is simulated over the tropical central Pacific and becomes significant from Apr1.

Based on the Gill response (Gill, 1980; Matsuno, 1966), the suppression of tropical African, Asian-Australian, and American monsoons could all excite the westerly anomaly of Kelvin wave response to their east side, thus the El Niño can develop through the Bjerknes feedback (Bjerknes, 1969). Our sensitivity experiments with aerosol forcing over different tropical lands show that El Niño response is simulated 1 year after the maximum aerosol forcing, while the response in the Land-Tropical African scenario is much stronger than the other scenarios (Figure 3b). The smaller land area and weaker monsoon suppression over tropical Asian-Australian could be one possible reason. The negative Niño3.4 response is simulated during year0 associated with the American monsoon suppression (Figure 3b), likely due to its close geophysical location with respect to tropical eastern Pacific. The easterly wind anomalies of Rossby wave in the west part of the Gill response could affect the eastern Pacific quickly, enhancing the upwelling and cooling the SST. During Year1, the Pacific warm Kelvin wave induced by the westerly wind anomalies in the east part of the Gill response develops and results in positive Niño3.4 response. The El Niño response in the Land-Tropical scenario is close to the El Niño responses averaged over individual regional scenarios (not shown), but much weaker to their linear sum (Figure 3b), suggesting non-linear ENSO variation to these regional or global volcanic forcings.

In consistent with the simulation in IPSL (Kh17), CESM also presents the leading role of tropical African cooling in exciting an El Niño response after tropical eruptions. Due to the large landmass of tropical Africa, the fast African cooling-induced land-sea thermal contrast suppresses the African monsoon and excites strong westerly wind anomaly over tropical Pacific, resulting in El Niño development through the Bjerknes feedback. Compared to IPSL results (Figure 5d of Kh17), CESM exhibits larger contribution from tropical Asian-Australian cooling to exciting an El Niño (Figure 3b).

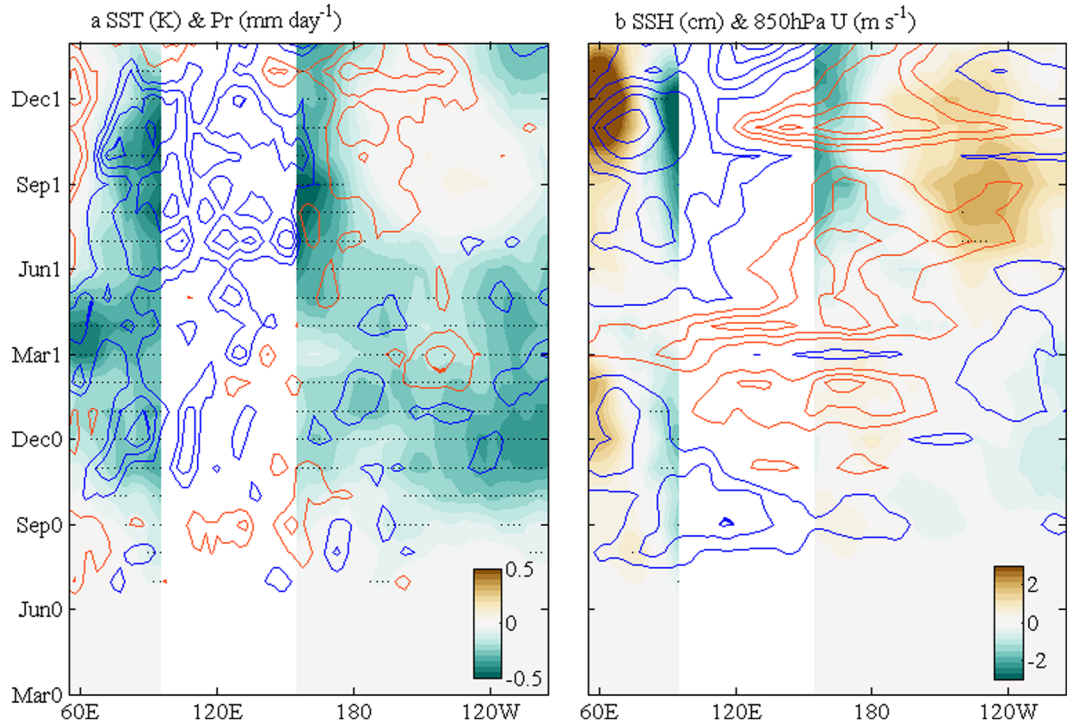

Figure 4. Role of ocean volcanic forcing in El Niño responses. (a) Hovmöller diagram of tropical (10°S–10°N) sea surface temperature (SST) (shading, K) and precipitation anomalies (contours, mm/day) that respond to aerosol forcing over ocean. Orange and blue contours denote positive and negative precipitation anomalies, respectively, and contour interval is 0.3 mm/day. Zero contour is not shown. Stippling and thick line denote anomalies significant at 95% confidence level based on the Student *t*-test. Panel (b) same as in panel (a) except for sea surface height (SSH: shading, cm) and 850 hPa zonal wind anomalies (contours, m/s). Contour interval is 0.3 m/s.

The ocean only volcanic forcing excites western Pacific El Niño-like tropical cooling, and it helps to enhance the El Niño response under the Global scenario (Figure 2). Significant cooling is simulated uniformly across tropical Pacific until Jun1 in the Ocean scenario, accompanied by negative precipitation anomalies from the Indian Ocean to the Pacific (Figure 4a). Significant positive Indian Ocean Dipole (IOD)-like sea surface height anomaly, associated with easterly wind anomalies and westward SST gradient over the tropical Indian Ocean and westerly wind anomalies over the tropical Pacific (Saji et al., 1999), is simulated from Nov0 (Figure 4b), although no western Pacific El Niño-like cooling is observed. Since Jun1, negative precipitation anomaly is simulated over the Warm Pool region, associated with positive IOD and El Niño-like cooling over Pacific. This result suggests that the Indian Ocean has a quicker response to the volcanic aerosol forcing than the Pacific Ocean does. The ocean thermostat which modulates the Pacific SST (Clement et al., 1996; D.-Z. Sun & Liu, 1996), seems to have a weak response to oceanic aerosol forcing.

The significant positive IOD response appears after Sep0, which tends to suppress the precipitation over the Warm Pool and excite westerly anomalies over the Pacific to excite the western Pacific El Niño-like cooling in Year1, although the development of IOD is interrupted during Spring1 (Figure 4b). Different from internal IOD which is basically locked to seasons from early summer to late fall (Saji et al., 1999), the IOD-like response to ocean aerosol forcing lasts to winter, especially in Year1. The Yoshida-Wyrtki jet, which brings warm water from the western equatorial Indian Ocean eastward during spring and fall when the monsoon breaks, is weakened due to strong easterly wind anomalies during late fall (Figure 4b). This could have enhanced the volcanic-forced IOD during late fall.

In IPSL, the western Pacific El Niño-like cooling is simulated during the first post-eruption winter under oceanic aerosol forcing (Figure 5b of Kh17). In CESM, however, a uniform Pacific cooling is simulated during the first post-eruption winter, while the western Pacific El Niño-like cooling only appears from Summer1 (Figure 4), suggesting a slower Pacific response in CESM than in IPSL. The larger amplitude of internal El Niño and weaker

western Pacific El Niño-like cooling under oceanic aerosol forcing in CESM than in IPSL may partly arise from the stronger radiative-SST feedback during an ENSO cycle in CESM (Chen et al., 2013).

4. Conclusions

Tropical volcanism has been found in observation, paleo-reconstruction, and modeling studies to trigger or increase the likelihood of El Niño's response. Various mechanisms have been proposed to explain the causal linkage, which can generally be categorized into oceanic related or land cooling dominated. We performed a set of sensitivity experiments to study relative roles of land and ocean cooling, by setting volcanic aerosol forcing of 1991 Pinatubo eruption over land and ocean separately, in the fully coupled CESM1.2. Our results present a significant El Niño response peaking 1 year after the maximum global aerosol forcing. The targeted sensitivity experiments show that the El Niño response is mainly triggered by aerosol forcing over tropical land, while aerosol forcing over ocean only excites western Pacific El Niño-like cooling, which likely enhances the El Niño response in the Global scenario. In the Land-Global scenario, the reduced land-sea thermal contrast induces monsoon suppression which in turn excites westerly anomalies on the east side to trigger an El Niño. Among different tropical land regions, volcanic-induced cooling and monsoon suppression in Africa is most efficient in exciting an El Niño.

Using different models and volcanic forcing strategies, our result and Kh17 both suggest the leading role of tropical African cooling and associated monsoon suppression in exciting an El Niño after tropical eruptions. We further find that the Indian Ocean responds faster to oceanic aerosol forcing than the Pacific. The positive IOD-like response, with a break during spring, persists to the second year, exciting the western Pacific El Niño-like cooling in Year1. Nevertheless, ocean cooling contributes relatively less to El Niño excitation than land cooling. Discrepancy between ours and Kh17 also suggests that models exhibit large inter-model bias in the role of ocean cooling, therefore more models to perform the same experiment as done by the VolMIP (Zanchettin et al., 2016) is encouraged.

Different from observation and paleo-reconstruction in which the El Niño is usually observed during the first boreal winter after tropical volcano eruptions (Khodri et al., 2017; Liu et al., 2018, 2022), CESM simulates the El Niño in the second winter, even in the Land scenario without the ocean cooling induced by aerosol forcing over the ocean. Here, we only simulated the volcano erupted in June and the forcing peaked in October, the El Niño therefore didn't have enough time to develop before the winter. Since the eruption season changes volcanic influence on ENSO (Stevenson et al., 2017), setting land-only or ocean-only aerosol forcing peaking at different months would be helpful to understand this observation-simulation bias. In this work we only focus on the ensemble mean without considering the role of internal variability, while the lack of an El Niño after 1883 Krakatau eruption calls further model investigation with land or ocean-only aerosol forcing together with different initial ocean conditions.

Conflict of Interest

The authors declare no conflicts of interest relevant to this study.

Data Availability Statement

The volcanic forcing data are available from Ammann et al. (2003) at https://doi.org/10.25921/ts5e-aw60. MATLAB version R2019a (available under MATLAB license at https://ww2.mathworks.cn/products/) and NCL version 6.6.2 (available at http://www.ncl.ucar.edu/Download/) are used for analysis. Different land and ocean volcanic aerosol forcings and part of the model outputs are available on https://doi.org/10.6084/m9.figshare.21586542. Other analytical scripts are available from the authors upon request.

Acknowledgments
This work was supported by the National Key Research and Development Program of China (2020YFA0608803) and the National Natural Science Foundation of China (Grant 41975107, 41875092, and 42005020). This paper is ESMC Contribution No. 397.

References

Adams, J., Mann, M. E., & Ammann, C. M. (2003). Proxy evidence for an El Niño-like response to volcanic forcing. *Nature*, *426*(6964), 274–278. https://doi.org/10.1038/nature02101

Ammann, C. M., Meehl, G. A., Washington, W. M., & Zender, C. S. (2003). A monthly and latitudinally varying volcanic forcing dataset in simulations of 20th century climate. *Geophysical Research Letters*, *30*(12), 1657. https://doi.org/10.1029/2003GL016875

Bellenger, H., Guilyardi, E., Leloup, J., Lengaigne, M., & Vialard, J. (2014). ENSO representation in climate models: From CMIP3 to CMIP5. *Climate Dynamics*, *42*(7), 1999–2018. https://doi.org/10.1007/s00382-013-1783-z

Bjerknes, J. (1969). Atmospheric teleconnections from the equatorial Pacific. *Monthly Weather Review*, *97*(3), 163–172. https://doi.org/10.1175/1520-0493(1969)097<0163:Atftep>2.3.Co;2

Capotondi, A., Deser, C., Phillips, A. S., Okumura, Y., & Larson, S. M. (2020). ENSO and Pacific decadal variability in the Community Earth System Model version 2. *Journal of Advances in Modeling Earth Systems*, *12*(12), e2019MS002022. https://doi.org/10.1029/2019MS002022

Chai, J., Liu, F., Xing, C., Wang, B., Gao, C., Liu, J., & Chen, D. (2020). A robust equatorial Pacific westerly response to tropical volcanism in multiple models. *Climate Dynamics*, *55*(11), 3413–3429. https://doi.org/10.1007/s00382-020-05453-6

Chen, L., Yu, Y., & Sun, D.-Z. (2013). Cloud and water vapor feedbacks to the El Niño warming: Are they still biased in CMIP5 models? *Journal of Climate*, *26*(14), 4947–4961. https://doi.org/10.1175/jcli-d-12-00575.1

Clement, A. C., Seager, R., Cane, M. A., & Zebiak, S. E. (1996). An ocean dynamical thermostat. *Journal of Climate*, *9*(9), 2190–2196. https://doi.org/10.1175/1520-0442(1996)009<2190:Aodt>2.0.Co;2

Clyne, M., Lamarque, J. F., Mills, M. J., Khodri, M., Ball, W., Bekki, S., et al. (2021). Model physics and chemistry causing intermodel disagreement within the VolMIP-Tambora Interactive Stratospheric Aerosol ensemble. *Atmospheric Chemistry and Physics*, *21*(5), 3317–3343. https://doi.org/10.5194/acp-21-3317-2021

D'Arrigo, R., Wilson, R., & Tudhope, A. (2009). The impact of volcanic forcing on tropical temperatures during the past four centuries. *Nature Geoscience*, *2*(1), 51–56. https://doi.org/10.1038/ngeo393

Dee, S. G., Cobb, K. M., Emile-Geay, J., Ault, T. R., Edwards, R. L., Cheng, H., & Charles, C. D. (2020). No consistent ENSO response to volcanic forcing over the last millennium. *Science*, *367*(6485), 1477–1481. https://doi.org/10.1126/science.aax2000

Gao, C., Robock, A., & Ammann, C. (2008). Volcanic forcing of climate over the past 1500 years: An improved ice core-based index for climate models. *Journal of Geophysical Research*, *113*(D23), D23111. https://doi.org/10.1029/2008JD010239

Gill, A. E. (1980). Some simple solutions for heat-induced tropical circulation. *Quarterly Journal of the Royal Meteorological Society*, *106*(449), 447–462. https://doi.org/10.1002/qj.49710644905

Handler, P. (1984). Possible association of stratospheric aerosols and El Nino type events. *Geophysical Research Letters*, *11*(11), 1121–1124. https://doi.org/10.1029/GL011i011p01121

Hawkins, E., Smith, R. S., Gregory, J. M., & Stainforth, D. A. (2016). Irreducible uncertainty in near-term climate projections. *Climate Dynamics*, *46*(11), 3807–3819. https://doi.org/10.1007/s00382-015-2806-8

Kay, J. E., Deser, C., Phillips, A., Mai, A., Hannay, C., Strand, G., et al. (2015). The Community Earth System Model (CESM) large ensemble project: A Community resource for studying climate change in the presence of internal climate variability. *Bulletin of the American Meteorological Society*, *96*(8), 1333–1349. https://doi.org/10.1175/bams-d-13-00255.1

Khodri, M., Izumo, T., Vialard, J., Janicot, S., Cassou, C., Lengaigne, M., et al. (2017). Tropical explosive volcanic eruptions can trigger El Niño by cooling tropical Africa. *Nature Communications*, *8*(1), 778. https://doi.org/10.1038/s41467-017-00755-6

Lim, H. G., Yeh, S. W., Kug, J. S., Park, Y. G., Park, J. H., Park, R., & Song, C. K. (2016). Threshold of the volcanic forcing that leads the El Niño-like warming in the last millennium: Results from the ERIK simulation. *Climate Dynamics*, *46*(11), 3725–3736. https://doi.org/10.1007/s00382-015-2799-3

Liu, F., Gao, C., Chai, J., Robock, A., Wang, B., Li, J., et al. (2022). Tropical volcanism enhanced the east Asian summer monsoon during the last millennium. *Nature Communications*, *13*(1), 3429. https://doi.org/10.1038/s41467-022-31108-7

Liu, F., Li, J., Wang, B., Liu, J., Li, T., Huang, G., & Wang, Z. (2018). Divergent El Niño responses to volcanic eruptions at different latitudes over the past millennium. *Climate Dynamics*, *50*(9), 3799–3812. https://doi.org/10.1007/s00382-017-3846-z

Liu, F., Xing, C., Li, J., Wang, B., Chai, J., Gao, C., et al. (2020). Could the recent Taal volcano eruption trigger an El Niño and lead to Eurasian warming? *Advances in Atmospheric Sciences*, *37*(7), 663–670. https://doi.org/10.1007/s00376-020-2041-z

Maher, N., McGregor, S., England, M. H., & Gupta, A. S. (2015). Effects of volcanism on tropical variability. *Geophysical Research Letters*, *42*(14), 6024–6033. https://doi.org/10.1002/2015GL064751

Mann, M. E., Cane, M. A., Zebiak, S. E., & Clement, A. (2005). Volcanic and solar forcing of the tropical Pacific over the past 1000 years. *Journal of Climate*, *18*(3), 447–456. https://doi.org/10.1175/jcli-3276.1

Matsuno, T. (1966). Quasi-geostrophic motions in the equatorial area. *Journal of the Meteorological Society of Japan. Series II*, *44*(1), 25–43. https://doi.org/10.2151/jmsj1965.44.1_25

McGregor, S., Khodri, M., Maher, N., Ohba, M., Pausata, F. S. R., & Stevenson, S. (2020). The effect of strong volcanic eruptions on ENSO. In *El Niño Southern Oscillation in a changing climate* (pp. 267–287).

McGregor, S., Timmermann, A., & Timm, O. (2010). A unified proxy for ENSO and PDO variability since 1650. *Climate of the Past*, *6*(1), 1–17. https://doi.org/10.5194/cp-6-1-2010

Ohba, M., Shiogama, H., Yokohata, T., & Watanabe, M. (2013). Impact of strong tropical volcanic eruptions on ENSO simulated in a coupled GCM. *Journal of Climate*, *26*(14), 5169–5182. https://doi.org/10.1175/jcli-d-12-00471.1

Pausata, F. S., Chafik, L., Caballero, R., & Battisti, D. S. (2015). Impacts of high-latitude volcanic eruptions on ENSO and AMOC. *Proceedings of the National Academy of Sciences of the United States of America*, *112*(45), 13784–13788. https://doi.org/10.1073/pnas.1509153112

Pausata, F. S. R., Karamperidou, C., Caballero, R., & Battisti, D. S. (2016). ENSO response to high-latitude volcanic eruptions in the Northern Hemisphere: The role of the initial conditions. *Geophysical Research Letters*, *43*(16), 8694–8702. https://doi.org/10.1002/2016GL069575

Pausata, F. S. R., Zanchettin, D., Karamperidou, C., Caballero, R., & Battisti, D. S. (2020). ITCZ shift and extratropical teleconnections drive ENSO response to volcanic eruptions. *Science Advances*, *6*(23), eaaz5006. https://doi.org/10.1126/sciadv.aaz5006

Predybaylo, E., Stenchikov, G., Wittenberg, A. T., & Osipov, S. (2020). El Niño/Southern Oscillation response to low-latitude volcanic eruptions depends on ocean pre-conditions and eruption timing. *Communications Earth & Environment*, *1*(1), 1–13. https://doi.org/10.1038/s43247-020-0013-y

Predybaylo, E., Stenchikov, G. L., Wittenberg, A. T., & Zeng, F. (2017). Impacts of a Pinatubo-size volcanic eruption on ENSO. *Proceedings of the National Academy of Sciences*, *122*(2), 925–947. https://doi.org/10.1002/2016JD025796

Robock, A. (2020). Comment on "No consistent ENSO response to volcanic forcing over the last millennium". *Science*, *369*(6509), eabc0502. https://doi.org/10.1126/science.abc0502

Saji, N. H., Goswami, B. N., Vinayachandran, P. N., & Yamagata, T. (1999). A dipole mode in the tropical Indian Ocean. *Nature*, *401*(6751), 360–363. https://doi.org/10.1038/43854

Sato, M., Hansen, J. E., McCormick, M. P., & Pollack, J. B. (1993). Stratospheric aerosol optical depths, 1850–1990. *Journal of Geophysical Research*, *98*(D12), 22987–22994. https://doi.org/10.1029/93JD02553

Stevenson, S., Fasullo, J. T., Otto-Bliesner, B. L., Tomas, R. A., & Gao, C. (2017). Role of eruption season in reconciling model and proxy responses to tropical volcanism. *Proceedings of the National Academy of Sciences*, *114*(8), 1822–1826. https://doi.org/10.1073/pnas.1612505114

Stevenson, S., Otto-Bliesner, B., Fasullo, J., & Brady, E. (2016). "El Niño like" hydroclimate responses to last millennium volcanic eruptions. *Journal of Climate*, *29*(8), 2907–2921. https://doi.org/10.1175/jcli-d-15-0239.1

Sun, D.-Z., & Liu, Z. (1996). Dynamic Ocean-atmosphere coupling: A thermostat for the tropics. *Science*, *272*(5265), 1148–1150. https://doi.org/10.1126/science.272.5265.1148

Sun, W., Liu, J., Wang, B., Chen, D., Liu, F., Wang, Z., et al. (2019). A "La Niña-like" state occurring in the second year after large tropical volcanic eruptions during the past 1500 years. *Climate Dynamics*, *52*(12), 7495–7509. https://doi.org/10.1007/s00382-018-4163-x

Taylor, K. E., Stouffer, R. J., & Meehl, G. A. (2012). An overview of CMIP5 and the experiment design. *Bulletin of the American Meteorological Society*, *93*(4), 485–498. https://doi.org/10.1175/bams-d-11-00094.1

Thomason, L. W., Ernest, N., Millán, L., Rieger, L., Bourassa, A., Vernier, J. P., et al. (2018). A global space-based stratospheric aerosol climatology: 1979–2016. *Earth System Science Data*, *10*(1), 469–492. https://doi.org/10.5194/essd-10-469-2018

Toohey, M., & Sigl, M. (2017). Volcanic stratospheric sulfur injections and aerosol optical depth from 500 BCE to 1900 CE. *Earth System Science Data*, *9*(2), 809–831. https://doi.org/10.5194/essd-9-809-2017

Wilson, R., Cook, E., D'Arrigo, R., Riedwyl, N., Evans, M. N., Tudhope, A., & Allan, R. (2010). Reconstructing ENSO: The influence of method, proxy data, climate forcing and teleconnections. *Journal of Quaternary Science*, *25*(1), 62–78. https://doi.org/10.1002/jqs.1297

Xing, C., Liu, F., Wang, B., Chen, D., Liu, J., & Liu, B. (2020). Boreal winter surface air temperature responses to large tropical volcanic eruptions in CMIP5 models. *Journal of Climate*, *33*(6), 2407–2426. https://doi.org/10.1175/jcli-d-19-0186.1

Yang, L., Gao, Y., Gao, C., & Liu, F. (2022). Climate responses to Tambora-size volcanic eruption and the impact of warming climate. *Geophysical Research Letters*, *49*(10), e2021GL097477. https://doi.org/10.1029/2021GL097477

Zanchettin, D., Bothe, O., Graf, H. F., Lorenz, S. J., Luterbacher, J., Timmreck, C., & Jungclaus, J. H. (2013). Background conditions influence the decadal climate response to strong volcanic eruptions. *Journal of Geophysical Research: Atmospheres*, *118*(10), 4090–4106. https://doi.org/10.1002/jgrd.50229

Zanchettin, D., Khodri, M., Timmreck, C., Toohey, M., Schmidt, A., Gerber, E. P., et al. (2016). The Model Intercomparison Project on the climatic response to Volcanic forcing (VolMIP): Experimental design and forcing input data for CMIP6. *Geoscientific Model Development*, *9*(8), 2701–2719. https://doi.org/10.5194/gmd-9-2701-2016

Zhu, F., Emile-Geay, J., Anchukaitis, K. J., Hakim, G. J., Wittenberg, A. T., Morales, M. S., et al. (2022). A re-appraisal of the ENSO response to volcanism with paleoclimate data assimilation. *Nature Communications*, *13*(1), 747. https://doi.org/10.1038/s41467-022-28210-1